12th International Congress on the Deterioration and Conservation of Stone
Columbia University, New York, 2012

MICRO-DESTRUCTIVE MAPPING OF SALT CRYSTALLIZATION IN STONE

Sevasti Modestou, Magdalini Theodoridou, Ioannis Ioannou and Revekka Fournari

Department of Civil and Environmental Engineering, University of Cyprus

Abstract

Micro-drilling and scratching are two micro-destructive techniques typically employed for the investigation of mechanical properties and the state of conservation of masonry materials, such as stone. In the current research, both aforementioned techniques have been used for the first time to map the distribution of salts in building stone in the laboratory, while micro-drilling was also applied in-situ. The results of the laboratory tests performed on limestone after cycles of impregnation with sodium sulfate confirm that these complimentary techniques can successfully detect the location of the salt front, as they respond to pore clogging by salt crystals by providing increased scratching/drilling resistance values. Drilling and scratching of duplicate samples treated with a hydrophobic product show the sensitivity of both techniques as they clearly detect changes to salt front location (i.e. cryptoflorescence) caused by surface treatments. Both techniques were also used to successfully characterize the difference in crystallization location and pattern in samples contaminated with magnesium sulfate. In-situ application of the micro-drilling test demonstrated its potential for use in the assessment of masonry salt weathering; the results suggest that this technique may, in fact, be useful as a preventive measure against salt damage.

Keywords: salt crystallization, micro-destructive techniques, DRMS, scratch tool, Na_2SO_4, $MgSO_4$, salt front mapping

1. Introduction

The crystallization of soluble salts is one of the most aggressive physical weathering processes affecting porous building materials (Goudie 1974), such as natural stone. Salt crystallization can detrimentally affect stone in terms of aesthetic, cultural, or economic value, as well as in terms of structural integrity. Thus, there is ample evidence of research work in the literature focusing on the weathering of natural stone caused by the crystallization of soluble salts (e.g. Goudie and Viles 1997; Rodriguez-Navarro and Doehne 1999; Ioannou and Hoff 2008; Espinosa-Marzal and Scherer 2010).

The position where salts crystallize is of utmost importance. When crystallization occurs on the surface of a stone (i.e. efflorescence), it is unsightly but harmless (except in the context of surface coatings or wall paintings). In contrast, crystallization occurring as sub- or crypto-florescence below the surface of a stone or within its porous network, is recognized by most researchers to be much more damaging (e.g. Benavente et al. 2004; Rodriguez-Navarro and Doehne 1999; Ioannou and Hoff 2008). Cryptoflorescence initially fills up pore space in a process known as pore clogging (Espinosa-Marzal and Scherer 2010); after a threshold volume of salt builds up, the crystals can exert a crystallization pressure great enough to overcome the tensile strength of the material and cause damage (Scherer 2004). The location of salt crystallization is affected by several factors, including the salts involved and their

properties, the host material and its properties, such as liquid transport behavior, and environmental conditions (Benavente et al. 2004; Ruiz-Agudo et al. 2007; Gomez-Heras and Fort 2007; Scherer 2004).

There are many techniques available which are suitable for determining or 'mapping' the location of salt crystallization within porous materials. In particular, several non-destructive imaging techniques have been applied for this purpose (e.g. Pel et al. 2000; Derluyn et al. 2008; Ruiz-Agudo et al. 2007; Ioannou et al. 2005). Such techniques are invaluable in salt crystallization research since their non-destructive nature makes it possible to use the same samples in a series of tests, enabling straightforward correlation of results. However, these techniques may not always be accessible to the wider community of conservators, archaeologists, engineers, and others working on salt crystallization issues, due to their often complex technical nature and relatively high cost. More importantly, none of these techniques can be used to map salts in-situ or within a wide range of sample dimensions.

In this paper, we propose the use of two novel micro- or semi-destructive techniques, the Drilling Resistance Measurement System (DRMS) and the scratch tool, as salt front mapping tools. Both techniques affect only a small amount of sample and can be applied to a range of specimens and dimensions. Furthermore, the DRMS was designed for in-situ application. Our work demonstrates the efficacy of both techniques as mapping tools and suggests that they may be used as alternatives to imaging techniques, since they have the ability to highlight localized changes in the pore structure of stone induced by salt crystallization.

2. Materials and Methodology

2.1 Materials

Lympia (LYM) stone, a relatively homogenous massive chalk named after its region of provenance, was selected for the laboratory tests. LYM is nearly exclusively composed of the foraminifera Globigerinidae (calcareous planktonic foraminifera) (Wilson and Ingham 1959). Powder X-Ray Diffraction (PXRD) analysis performed on fresh samples indicated nearly 100 per cent calcite with a trace of quartz. LYM primarily exhibits intragranular porosity; pores are mainly observed within the cavities of the foraminifera.

The physical and mechanical properties of freshly quarried LYM stone were determined by standardized tests. Mercury intrusion porosimetry (MIP) was also performed to investigate its pore structure characteristics. The results are summarized in Table 1. As shown in the table, the most remarkable properties of LYM include its relatively high porosity (ca. 43 per cent) and capillary absorption coefficient (140.5 $g/m^2s^{1/2}$).

Table 1. Physico-mechanical characteristics of Lympia Stone.

Mercury Porosimetry Results*		**Standardized Test Results**		
Bulk density (kg/m^3)	1535	Apparent density (kg/m^3)	1551	EN 1936
Open porosity (%)	42.6	Open porosity (%)	42.8	EN 1936
Average pore throat diameter (μm)	0.227	Capillary absorption coefficient ($g/m^2s^{1/2}$)	140.5	EN 1925
		Flexural strength (MPa)	6.0	EN 12372

* *Average of two samples*

2.2 Idealized mapping sample preparation

Idealized mapping samples (7x7x7 cm cubes of LYM) were prepared in order to initially assess the ability of the micro-destructive techniques to map the salt front. The samples were sealed with epoxy resin on their vertical sides to approximate one-dimensional liquid transport and thus simplify analysis (e.g. Ioannou et al. 2005; Derluyn et al. 2008; Espinosa-Marzal and Scherer 2010). Samples were prepared in pairs, one of which was treated on its upper face with sodium methylsiliconate water repellent (CH_5NaO_3Si, 5% wt/wt). The repellent was brushed on in two coats and the samples were allowed to air dry for 24 hours before oven drying at 70°C. This treatment cures in surface pores to form a coating which is permeable to water vapour but repels water in liquid form (Ioannou and Hoff 2008). The purpose of its application was to enforce cryptoflorescence to occur, thus effectively changing the position of the salt crystallization front between the two cubes in each pair.

0.435 M Na_2SO_4 or $MgSO_4$ salt solutions were imbibed into the cubes from the bottom side until enough salt was absorbed to theoretically fill approximately 2 mm of pore space with crystals. The bases of the cubes were sealed to force evaporation during drying to occur only through the upper faces. The salt, drying temperature, and number of crystallization cycles each pair of samples was subjected to is shown in Table 2. Sorptivity tests using heptane were performed before and after salt contamination to detect changes in the pore system of the samples. Analysis of the data was performed according to Gummerson et al. (1980), with the data plotted as i (the volume of liquid absorbed per unit of absorption surface area, [mm]) versus the square root of time [$min^{1/2}$]. The relationship i / f (where f is porosity) was used to determine the spatial location of any changes in sorptivity.

Table 2. Cycles of crystallization and drying temperature.

Salt	Temperature	No. of Cycles
0.435 M Na_2SO_4	70°C	3
0.435 M $MgSO_4$	70°C	2

2.3 Micro-destructive techniques

The DRMS is probably best known for assessing the state of weathering of masonry and the effects of surface treatments such as consolidants (Pamplona et al. 2007). The scratch tool has been used primarily to assess mechanical properties (e.g. Detournay and Defourny 1992; Richard et al. 1998), although recently it has also been applied to problems in conservation (e.g. Dagrain et al. 2012). A detailed explanation of both techniques can be found in Theodoridou et al. (2012).

In this research, both the DRMS and the scratch tool were used to locate the position of the salt front, after each cycle of salt contamination and drying, in the idealized samples described above. Scratching was performed at a rate of 10 mm/s with a sharp diamond cutter inclined backwards at 15°. Successive scratches were employed, beginning at 0.10 mm depth and incrementally increasing by 0.05 mm to a maximum depth of 0.40 mm. The graphs produced from each individual scratch were averaged to produce a mapping pattern. For simplicity of data presentation, only the tangential component of force recorded by the scratch device was selected for use here.

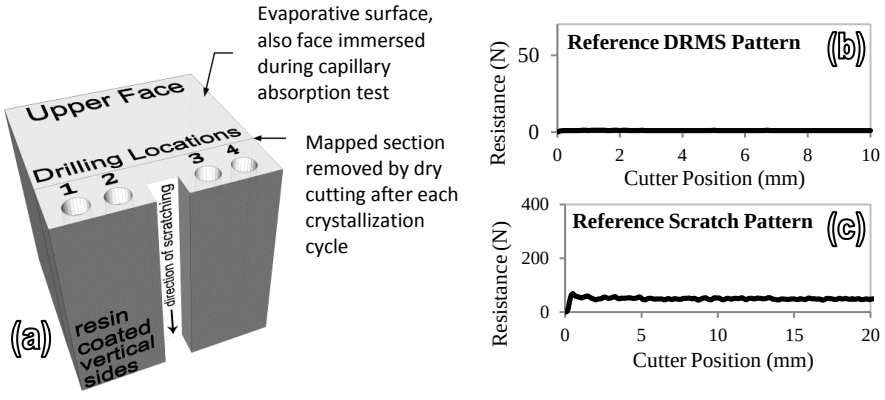

Figure 1. (a) Orientation of sample during testing and location of micro-destructive tests. (b) Reference DRMS pattern. (c) Reference scratch pattern.

Following scratching, four DRMS measurements were performed (drilling speed 600 rpm with a 10 mm/min penetration rate), two to either side of the scratch groove. A 5 mm diameter diamond drill bit was used and the total penetration depth was 10 mm, unless otherwise noted. Rock powder produced during drilling was collected for PXRD analysis. The DRMS mapping patterns were not averaged due to the fact that slight variations were detected in salt front position from point to point throughout the sample. Figure 1a shows the idealized mapping sample set up and the location of micro-destructive testing. After mapping was performed, the affected portion of the samples was removed by dry cutting and the surface was re-sealed with resin.

A sample of LYM which had not undergone any salt contamination was scratched and drilled to generate reference patterns for comparison (Figure 1(b,c)). The reference patterns show a smooth plateau of resistance to the cutting tool (N) versus cutter position (mm) in both cases.

2.4 In-Situ Experiments

The portable DRMS was also used to perform in-situ micro-drilling on a 110 year old LYM stone masonry church. The same operating conditions were employed for in-situ testing as for the laboratory tests. Areas for salt mapping were selected based on visible damage, surface moisture content and accessibility. Rock powder was collected during drilling for PXRD analysis to determine the presence of salts and to estimate their concentration. The results presented here are from one single block of masonry (LSB) which showed variable weathering over its face (Figure 2).

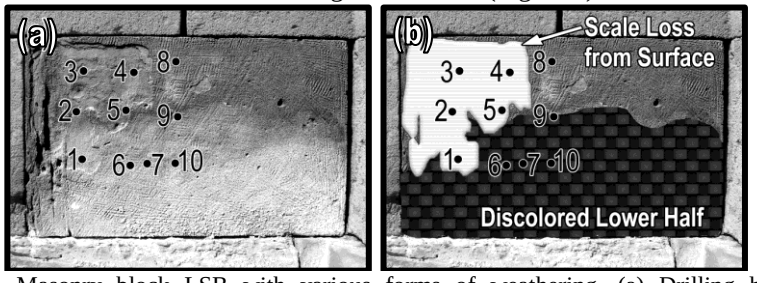

Figure 2. Masonry block LSB with various forms of weathering. (a) Drilling holes and appearance. (b) Weathering forms; at hole 1 both types of weathering exist.

3. Results and Discussion

From the results of micro-destructive mapping (Figure 3), one can observe a clear peak in both drilling and scratching resistance patterns in the Na_2SO_4 contaminated samples, in comparison to the reference patterns. This peak appears immediately after the first crystallization cycle. In the untreated samples, the peak is located directly at the evaporative surface. In contrast, repellent treated samples show a wider peak located just below their surface. The DRMS patterns indicate that this peak is between approximately 1 and 3 mm below the surface of the material, depending on the exact location of the drill hole. The scratch patterns indicate that the peak begins approximately 2 mm below the surface in treated samples; there is no variation since scratching was performed at essentially the same position. The similarity in peak position between the two methods supports the validity of the results.

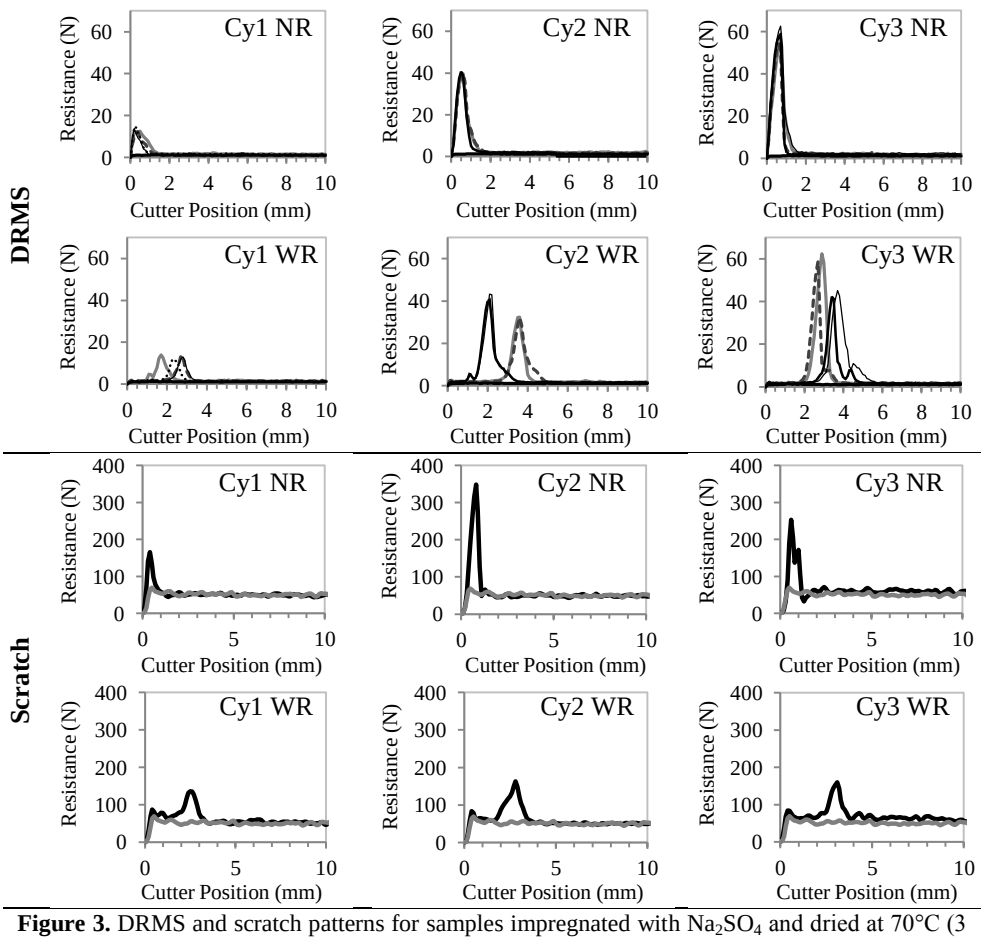

Figure 3. DRMS and scratch patterns for samples impregnated with Na_2SO_4 and dried at 70°C (3 cycles). DRMS: ▬ hole 1;▪▪▪▪ hole 2;····· hole 3; ▬ hole 4; ▬ reference pattern. Scratch: ▬ salt contaminated pattern; ▬ reference pattern. Cy: cycle; NR: no repellent; WR: with repellent. The origin corresponds to the upper face; cutting was performed perpendicular to this face.

The observations from the mapping patterns are supported by stereoscope observations of the samples (Figure 4). Salt has clearly crystallized on the surface of the untreated specimen, while the treated specimen appears clean (Figure 4(a,b)). Furthermore, within the scratch groove of the repellent treated samples, a linear feature could be observed after the first crystallization cycle (Figure 4(c)), approximately 2.5 mm below and parallel to the evaporative surface. This is a further confirmation of the location of the salt front in the repellent treated samples. No such line is observed in the untreated samples, and no such feature was observed in the uncontaminated material.

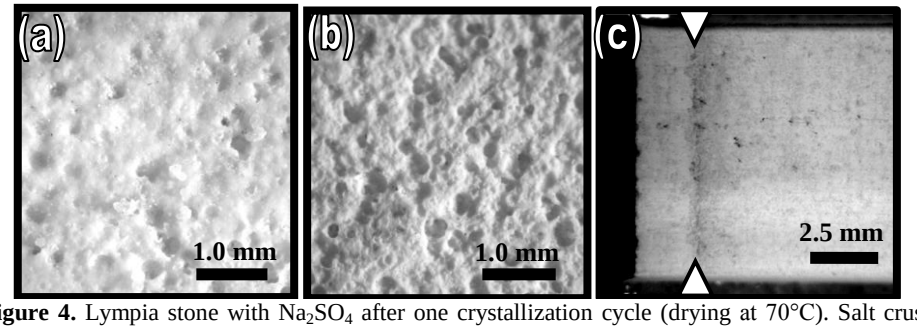

Figure 4. Lympia stone with Na_2SO_4 after one crystallization cycle (drying at 70°C). Salt crust appears on the upper face of the untreated sample (a) while the water repellent treated sample appears clean (b). (c) Linear feature (arrows) likely due to salt observed in the scratch groove of the repellent treated sample. Scratching left to right. Source: Modestou et al. (2011).

3.1 Capillary absorption tests

Early-time (25 min) sorptivity results for Na_2SO_4 contaminated samples are presented in Table 3. From these, it is clear that the addition of salt significantly decreases the sorptivity. The increase observed at cycle 3 for LYM WR sample could be attributed to internal microcracking. Unfortunately, to confirm this, further work, such as imaging experiments (i.e. x-ray tomography) should be carried out.

Table 3. Changes to sample sorptivity ($mm/min^{1/2}$) caused by Na_2SO_4 crystallization.

Salt	Sample[+]	Initial	Cycle 1	Cycle 2	Cycle 3
Na_2SO_4	LYM WR	1.353	0.074	0.036	0.127
	LYM NR	1.316	0.129	0.038	0.035

[+]LYM: Lympia stone; WR: with repellent, NR: no repellent.

Figure 5 shows a graph of the original sorptivity compared to the sorptivity after one cycle with Na_2SO_4 for the repellent treated sample dried at 70°C. From this graph, it is clear that there is a major change in the sorptivity of the material before and after the crystallization of Na_2SO_4. Furthermore, there is a change in the slope of the line of the second graph (i.e. after the crystallization cycle) at time 8.75 $min^{1/2}$. This suggests that the changes to the pore network of the sample are localized. The location of the change in sorptivity was determined to be 2.45 mm from the surface of the sample (calculation superimposed on graph, Figure 5). The only change to the material which could cause such a change in sorptivity is contamination with salt; therefore, this location should correspond to the base of the salt front. As such, the distance calculated should also match the point in the patterns immediately after the peak in resistance. This is indeed

the case and the aforementioned result correlates quite well to the expected point in the micro-destructive mapping patterns (see Figure 5, Cy1 WR). A similar result was found for all samples, with the change in sorptivity occurring much closer to the evaporative surface in the untreated specimens.

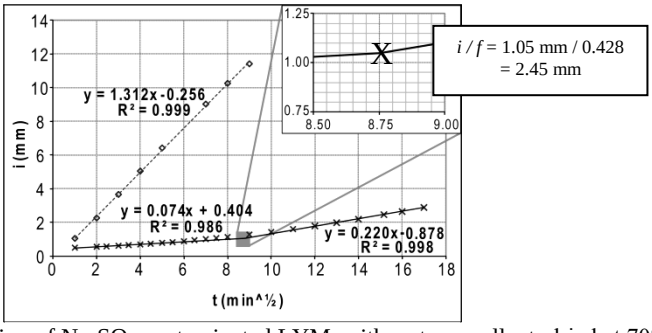

Figure 5. Capillary absorption of Na_2SO_4 contaminated LYM, with water repellent, dried at 70°C. Dashed line: original sorptivity; solid line: sorptivity after one contamination cycle. Insert: magnification at location of sorptivity change (X = i / f = 2.45 mm, see text). Reproduced from Modestou, 2012.

Overall, the results strongly support the case that the location of salt crystallization can be precisely mapped by micro-drilling and scratching. This is likely due to local changes in the pore system caused by pore clogging. A higher concentration of salt within the same volume of porous material should equate to a decrease in void or pore space, leading to a local increase in the resistance of the material to cutting. The general increase in peak magnitude seen in subsequent cycles likely indicates that pore clogging is increasing and the salt front is becoming denser. Following this interpretation, the micro-destructive results indicate that Na_2SO_4 crystallizes in a thin localized band at or near the material surface, in a position coinciding with the drying or evaporation front. This observation is consistent with the literature (e.g. Ioannou et al. 2005; Derluyn et al. 2008). Also, the results emphasize the tendency of repellents to cause cryptoflorescence to occur, leading to more severe damage in salt contaminated materials.

3.2 Crystallization with $MgSO_4$

The mapping patterns for samples contaminated with $MgSO_4$ are shown in Figure 6. In comparison to those obtained from Na_2SO_4 contaminated samples, definite peaks are not observed here until after the second cycle. Furthermore, the peaks which appear after the second cycle indicate that $MgSO_4$ has crystallized beneath the surface regardless of whether or not repellent was applied to the sample. This suggests that $MgSO_4$ moves much slower towards the drying surface than Na_2SO_4. The reason for this lies within the solution properties of $MgSO_4$ which has greater density and higher viscosity in comparison to Na_2SO_4; such properties lead to a tendency for crystallization to occur further away from the surface, since motion of the solution by capillary flow upon drying is slower (Ruiz-Agudo et al. 2007). It is worth noting that the repellent treated sample cracked extensively after the second cycle; this is an indication that $MgSO_4$ is more damaging than Na_2SO_4 under the conditions used in these experiments.

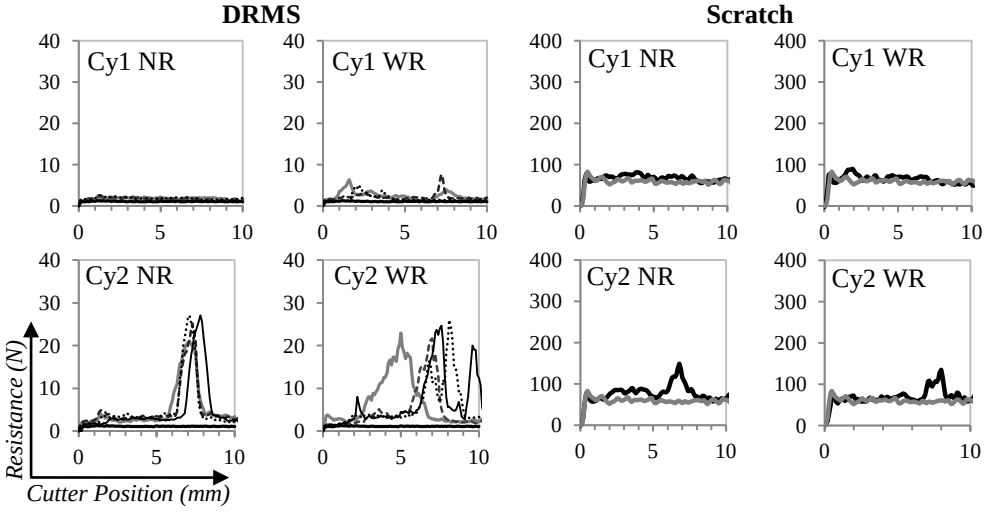

Figure 6. DRMS and scratch patterns for samples contaminated with $MgSO_4$ and dried at 70°C (2 cycles). DRMS: ▬ hole 1; ▪▪▪ hole 2; ····· hole 3; ▬ hole 4; ▬ reference pattern. Scratch: ▬ salt contaminated pattern; ▬ reference pattern. Cy: cycle; NR: no repellent; WR: with repellent. The origin corresponds to the upper surface or drying surface of the samples; cutting was performed perpendicular to this surface.

3.3 In-situ results

The archetype of a peak at the beginning of the cutting pattern, followed by a relatively smooth plateau, was again observed during the in-situ drilling for some of the holes (Figure 7(a)). This indicates that most of the salts affecting the church wall block concentrate at the surface of the material. The patterns show that micro-drilling performed on the discoloured area of LSB (holes 1, 6, 7, 9, and 10) corresponded to higher peak force values (Table 4). This was the first indication that the discoloured section of the block may in fact correspond to salt concentration in and/or on the stone. Holes on the section suffering from material loss (holes 2, 3, 4, 5, and 8) showed little or no peak, likely reflecting the tendency of surface scale loss to also remove salts.

Table 4. Peak force (PF) and gypsum concentration (GC) for each DRMS hole in LSB (see Fig. 2 for hole positions). n/a: failure to collect sample.

Hole	PF (N)	GC (%)	Hole	PF (N)	GC (%)
1	23.80	7.9	2	8.39	3.5
6	29.45	11.0	3	5.57	1.0
7	30.94	n/a	4	5.19	2.2
9	23.53	4.3	5	11.13	5.2
10	28.60	12.3	8	5.31	2.8

PXRD of the powder collected during drilling indicated gypsum in addition to calcite and quartz. Gypsum is known to occur in limestone as a product of weathering (Halsey et al. 1995). Semi-quantitative analysis of the PXRD data indicated a good correlation between gypsum concentration and peak force from the DRMS patterns

(Figure 7(b)). From this trend, again it can be inferred that pore clogging by salt crystallization is the mechanism leading to the increased force seen in the cutting patterns. The main drawback of this technique is that another form of analysis must be used to determine what, if any, salts are present; advances in in-situ Raman spectroscopy could be one solution (e.g. Lopez-Arce et al. 2011).

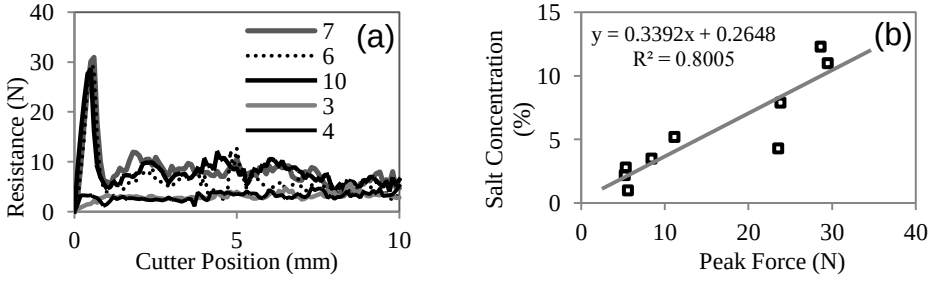

Figure 7. In-situ DRMS on LSB. (a) Selected patterns (see Figure 2 for hole location). (b) Relationship between peak force and gypsum concentration.

4. Conclusions

The Drilling Resistance Measuring System (DRMS) and scratch tool demonstrated clear potential to map the location of the salt crystallization front through purpose-designed laboratory tests in natural stone. The cutting patterns from the salt contaminated samples definitively indicate a localized increase in the force required to cut at the salt front. This increase is attributed to pore clogging by salt crystallization. The efficacy of the two techniques in mapping the salt front was further confirmed by the difference noted in the position of crystallization in water repellent treated and untreated samples, as well as by changes to material sorptivity after salt contamination at precise locations matching the locations of the peaks in resistance to cutting/drilling.

Micro-drilling also divulged important information about the modus and stage of weathering in stone masonry in-situ. Of particular significance is the observation that areas which appear relatively less weathered may be contaminated with a high proportion of salt. Although other analyses must be performed to determine the identity and concentration of compounds present (e.g. PXRD), DRMS may provide a relatively quick and easy assessment of the existence and location of salt crystallization in-situ. Such information could be vital to professionals dealing with salt crystallization problems in structures; more importantly, there is potential to assess salt crystallization in-situ before permanent damage even occurs.

ACKNOWLEDGEMENTS: This work was co-funded by the European Regional Development Fund and the Republic of Cyprus through the Research Promotion Foundation (Projects ΕΠΙΧΕΙΡΗΣΕΙΣ/ΣΥΛΛΟ/0308/02 and ΝΕΑ ΥΠΟΔΟΜΗ/ΝΕΚΥΠ/0308/17).

References

Benavente, D., Garcia del Cura, M. A., Garcia-Guinea, J., *et al*. 2004. Role of pore structure in salt crystallization in unsaturated porous stone. *Journal of Crystal Growth*. **260**[3-4]: 532-44.

Derluyn, H., Poupeleer, A. S., Van Gemert, D., *et al*. 2008a. Salt crystallization in hydrophobic porous materials. Proceedings of *Hydrophobe V Conference*, April 15-16, 2008.

Espinosa-Marzal, R. M. and Scherer, G. W. 2010. Mechanisms of damage by salt. *Geological Society, London, Special Publications*. **331**[1]: 61-77.

Gomez-Heras, M., and Fort, R. 2007. Patterns of halite (NaCl) crystallization in building stone conditioned by laboratory heating regimes. *Environmental Geology*. **52**[2]: 259-67.

Goudie, A. S. 1974. Further experimental investigation of rock weathering by salt and other mechanical processes. *Zeitschriftfur Geomorphologie Supplementband*. **21**, 1-12.

Goudie, A. S., and Viles, H. 1997. *Salt Weathering Hazards*. Chinchester: Wiley.

Gummerson, R. J., Hall, C., and Hoff, W. D. 1980. Water movement in porous building materials II. Hydraulic suction and sorptivity of brick and other masonry materials. *Building and Environment*. **15**[3]: 101-8.

Halsey, D. P., Dews, S. J., Mitchell, D. J., *et al*. 1995. Real time measurements of sandstone deterioration: a microcatchment study. *Building and Environment*. **30**[3]: 411-17.

Ioannou, I., and Hoff, W. D. 2008. Water repellent influence on salt crystallisation in masonry. *Proceedings of the ICE - Construction Materials*. **161**[1]: 17-23.

Ioannou, I., Hall, C., Hoff, W. D., *et al*. 2005. Synchrotron radiation energy-dispersive X-ray diffraction analysis of salt distribution in Lépine limestone. *The Analyst*. **130**[7]: 1006-8.

López-Arce, P., Zornoza-Indart, A., Vázquez-Calvo, C., *et al*. 2011. Evaluation of Portable Raman for the Characterization of Salt Efflorescences at Petra, Jordan. *Spectroscopy Letters*. 44, 505-10.

Modestou, S. 2012. *Salt weathering in natural stone and micro-destructive mapping of the crystallization front*. M.Sc. Thesis, University of Cyprus.

Modestou, S., Ioannou, I., and Theodoridou, M. 2011. Salt distribution mapping in natural building and decorative stones. In: Leung, C., and Wan, K. T. (Eds.) *Advances in Construction Materials through Science and Engineering* (p. 110, abstract; full text in electronic proceedings). Bagneux, France: RILEM.

Pamplona, M., Kocher, M., Snethlage, R., *et al*. 2007. Drilling resistance: overview and outlook. *Zeitschriftder Deutschen Gesellschaft für Geowissenschaften*. **158**[3]: 665-79.

Pel, L., Kopinga, K., and Kaasschieter, E. F. 2000. Saline absorption in calcium-silicate brick observed by NMR scanning. *Journal of Physics D: Applied Physics*. **33,** 1380-5.

Rodriguez-Navarro, C. and Doehne, E. 1999. Salt weathering: influence of evaporation rate, supersaturation and crystallization pattern. *Earth Surface Processes and Landforms*. **24**[3]: 191-209.

Ruiz-Agudo, E., Mees, F., Jacobs, P., *et al*. 2007. The role of saline solution properties on porous limestone salt weathering by magnesium and sodium sulfates. *Environmental Geology*. **52**[2]: 269-81.

Scherer, G. W. 2004. Stress from crystallization of salt. *Cement and Concrete Research*. **34**[9]: 1613-24.

Theodoridou, M., Dagrain, F., and Ioannou, I. 2012. Correlation of stone properties using standardized methodologies and non-standardized micro-destructive techniques. Proceedings of the *12th International Conference on the Deterioration and Conservation of Stone* (this volume).

Wilson, R. A. M., and Ingham, F. T. 1959. *The Geology of the Xeros-Troodos Area, with an Account of the Mineral Resources. Memoir No. 1*. Nicosia: Geological Survey Department, Republic of Cyprus.